Supplementary Information

Pyrimido[4,5-*g*]quinazoline-4,9-dione as a new building block for constructing polymer semiconductors with high sensitivity to acids and hole transport performance in organic thin film transistors

Jesse Quinn, Chang Guo, Bin Sun, Adrian Chan, Yinghui He, Edward Jin, and Yuning Li*

Department of Chemical Engineering, University of Waterloo, 200 University Avenue West, Waterloo, Ontario, Canada N2L 3G1

E-mail: yuning.li@uwaterloo.ca

Additional data

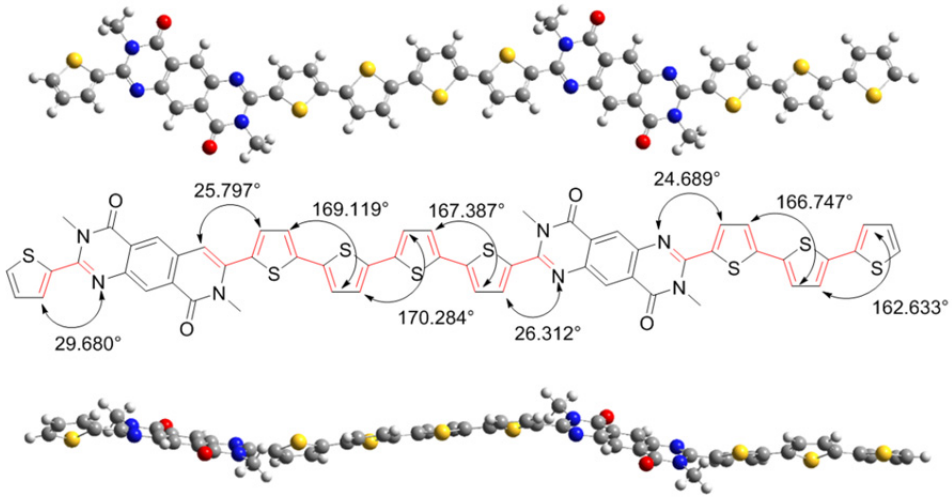

Fig. S1 The optimized geometry and dihedral angles of the **PQ2T-BT-Me** dimer through Gaussian 09 Revision D.01[1] using the functional B3LYP and the basis set 6-31G(d) under tight convergence.

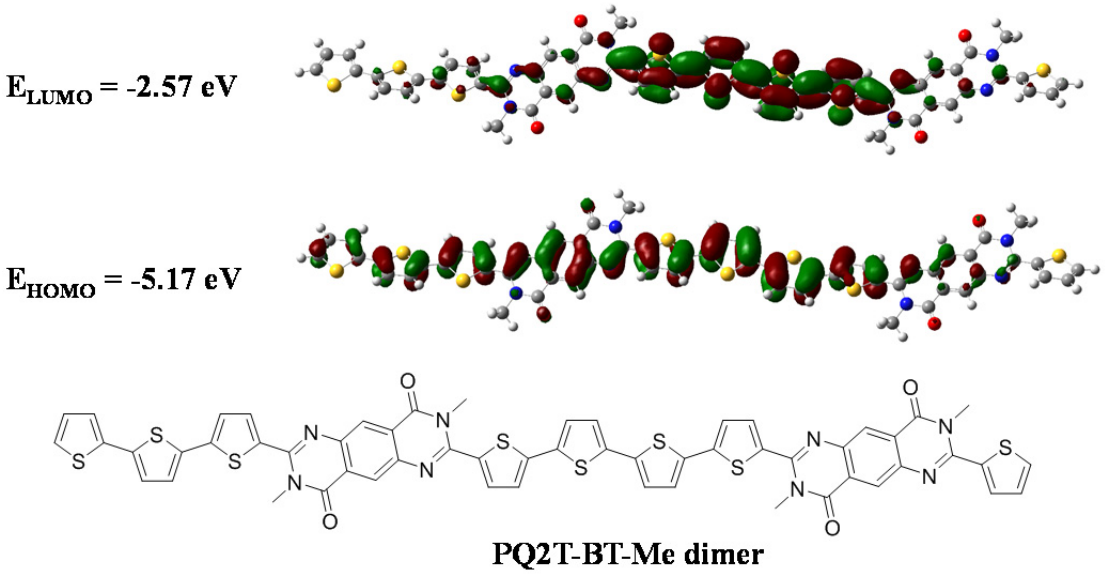

Fig. S2 The optimized LUMO and HOMO wavefunction distributions of the **PQ2T-BT-Me** dimer through Gaussian 09 Revision D.01[1] using the functional B3LYP and the basis set 6-31G(d) under tight convergence .

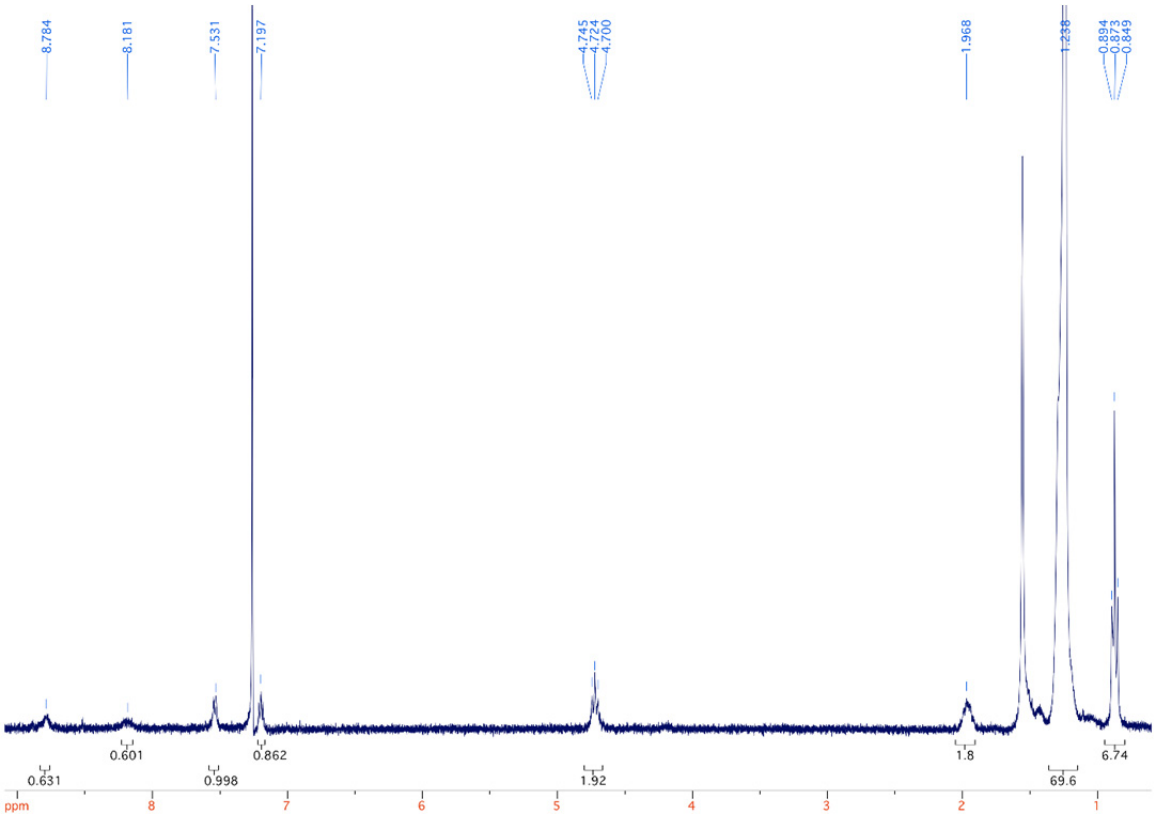

Fig. S3 300 MHz ^{1}H NMR spectrum for 3,8-bis(4-octadecyldocosyl)-2,7-di(thiophen-2-yl)-3,8-dihydropyrimido[4,5-*g*]quinazoline-4,9-dione (**PQ2T-40**) in $CDCl_3$.

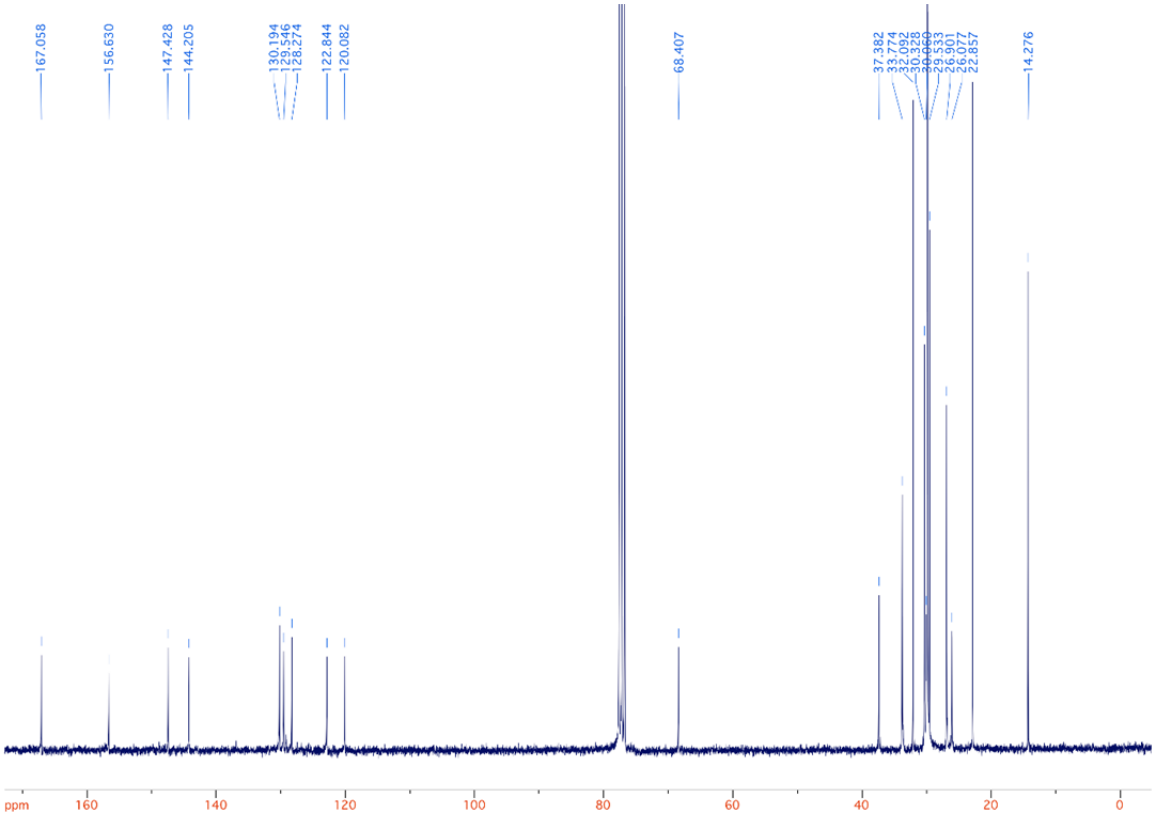

Fig. S4 75 MHz ^{13}C NMR spectrum for 3,8-bis(4-octadecyldocosyl)-2,7-di(thiophen-2-yl)-3,8-dihydropyrimido[4,5-*g*]quinazoline-4,9-dione (**PQ2T-40**) in $CDCl_3$.

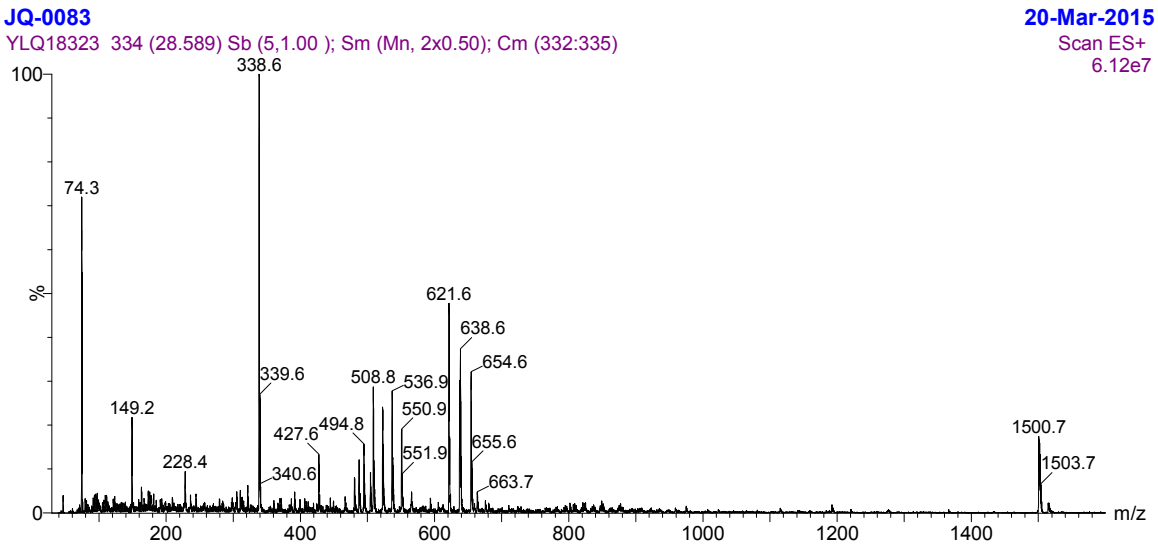

Fig. S5 The MS (ESI+) [M+H]+ spectra for 3,8-bis(4-octadecyldocosyl)-2,7-di(thiophen-2-yl)-3,8-dihydropyrimido[4,5-*g*]quinazoline-4,9-dione (**PQ2T-40**).

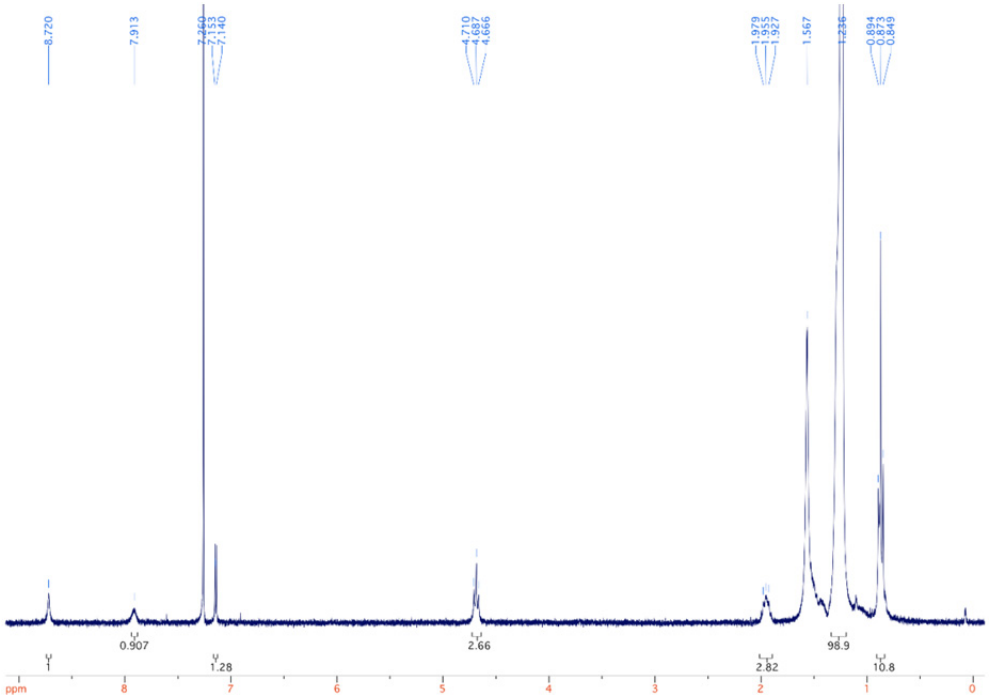

Fig. S6 300 MHz ^{1}H NMR spectrum for 2,7-bis(5-bromothiophen-2-yl)-3,8-bis(4-octadecyldocosyl)-3,8-dihydropyrimido[4,5-*g*]quinazoline-4,9-dione (**PQ2T-Br-40**) in $CDCl_3$.

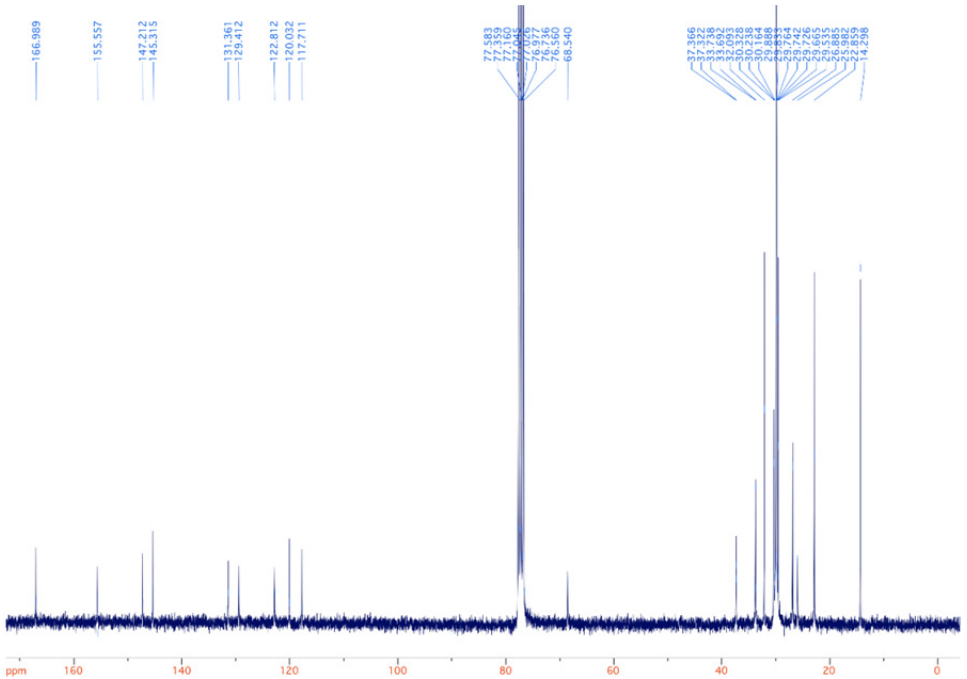

Fig. S7 75 MHz ^{13}C NMR spectrum for 2,7-bis(5-bromothiophen-2-yl)-3,8-bis(4-octadecyldocosyl)-3,8-dihydropyrimido[4,5-*g*]quinazoline-4,9-dione (**PQ2T-Br-40**) in $CDCl_3$.

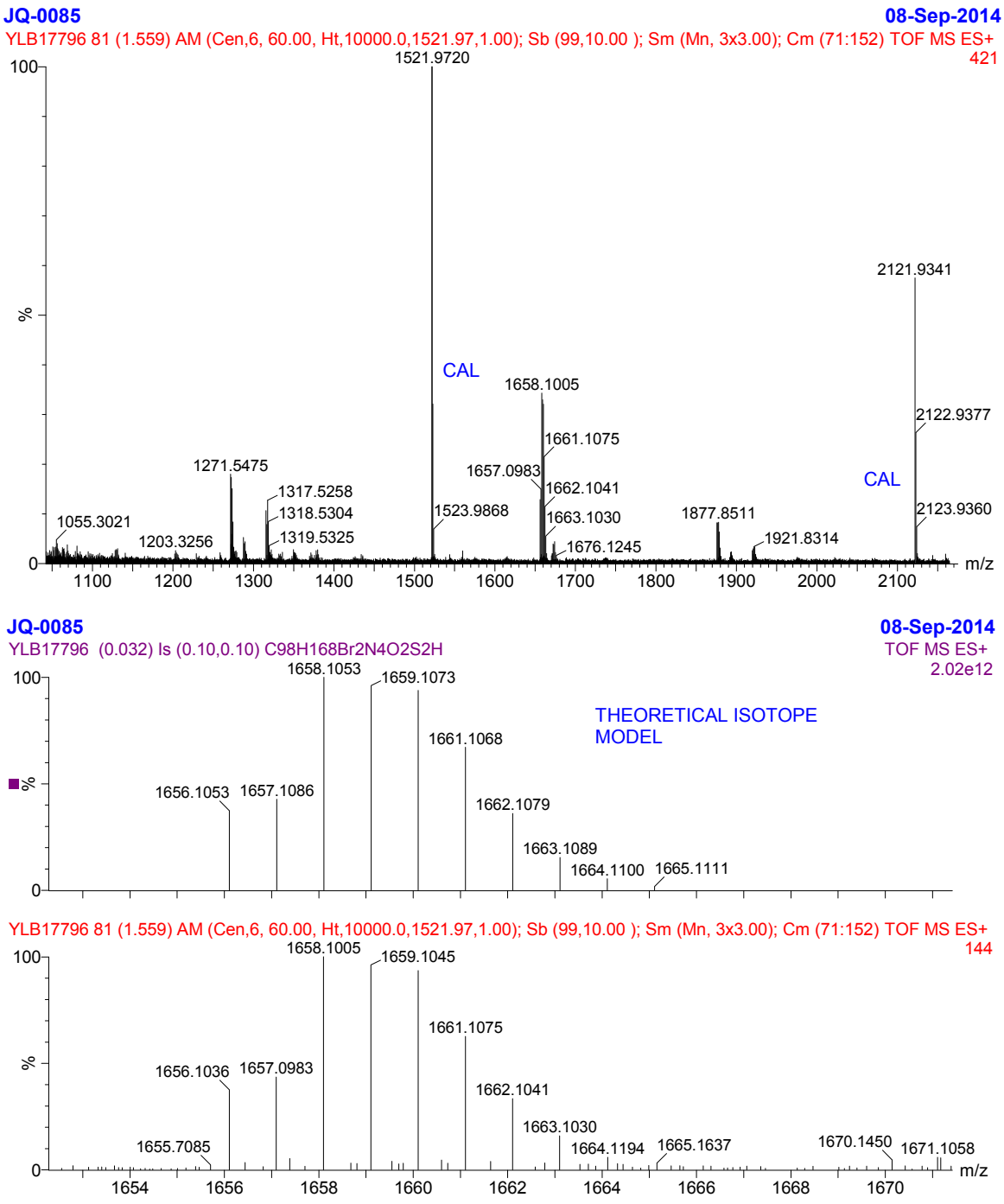

Fig. S8 The HR-MS (ESI+) (M+H)+ spectra for 2,7-bis(5-bromothiophen-2-yl)-3,8-bis(4-octadecyldocosyl)-3,8-dihydropyrimido[4,5-*g*]quinazoline-4,9-dione (**PQ2T-Br-40**).

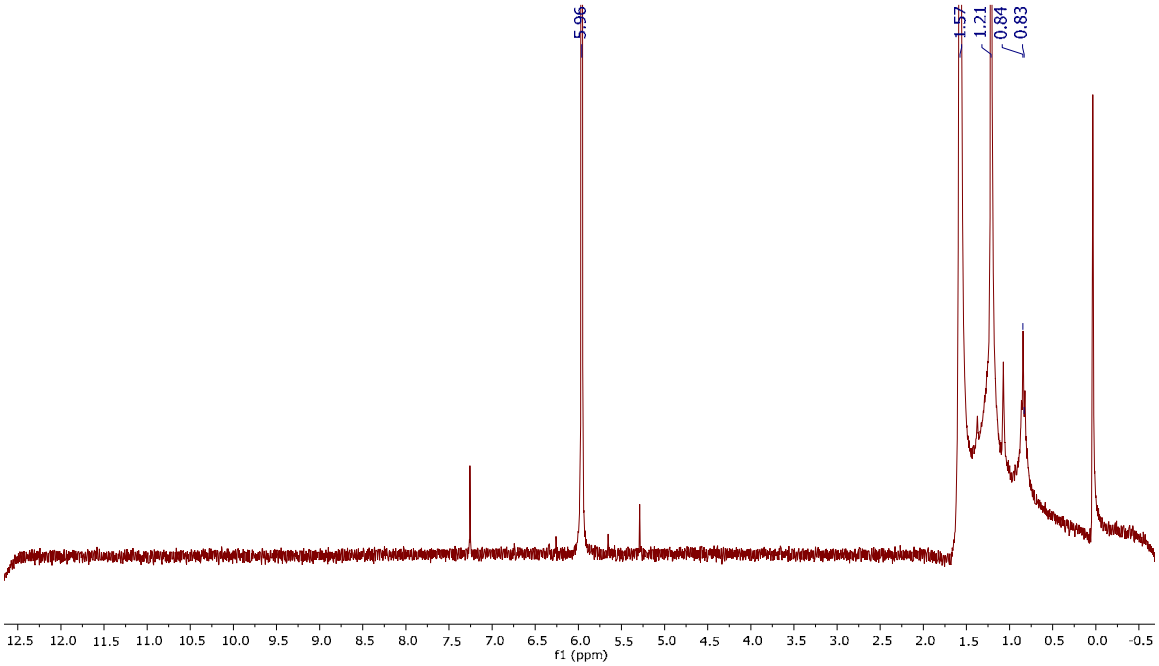

Fig. S9 300 MHz ^{1}H NMR spectrum for **PPQ2T-BT-24** in 1,1,2,2-tetrachloroethane-d_2.

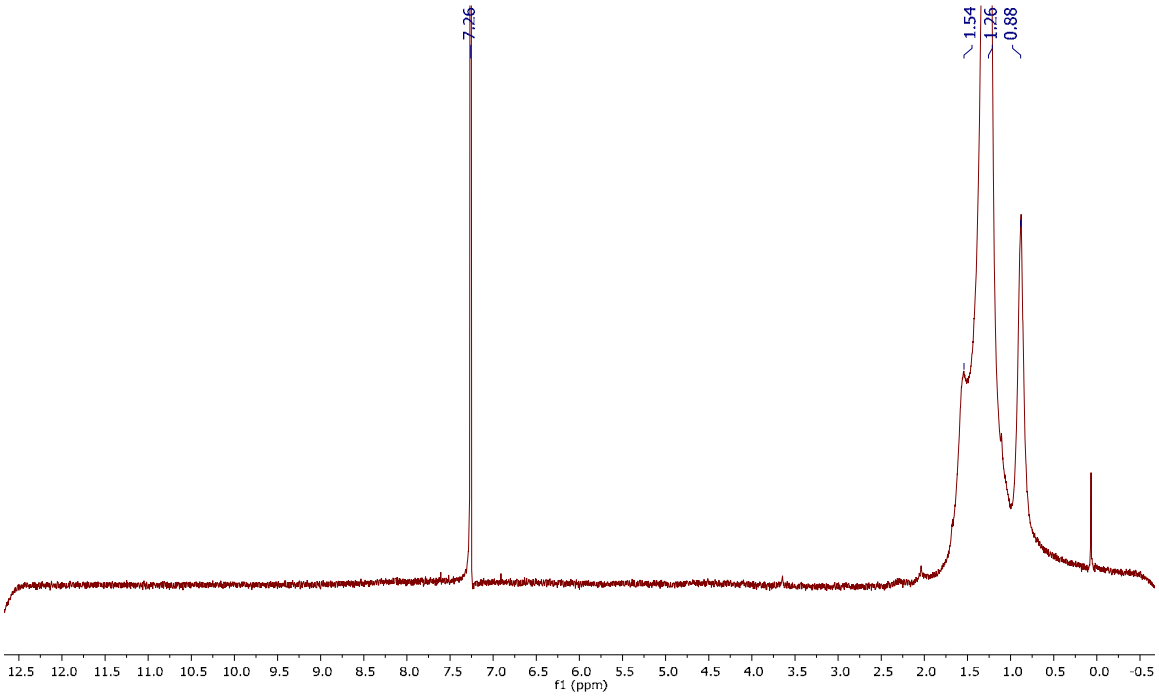

Fig. S10 300 MHz ^{1}H NMR spectrum for **PPQ2T-BT-40** in $CDCl_3$.

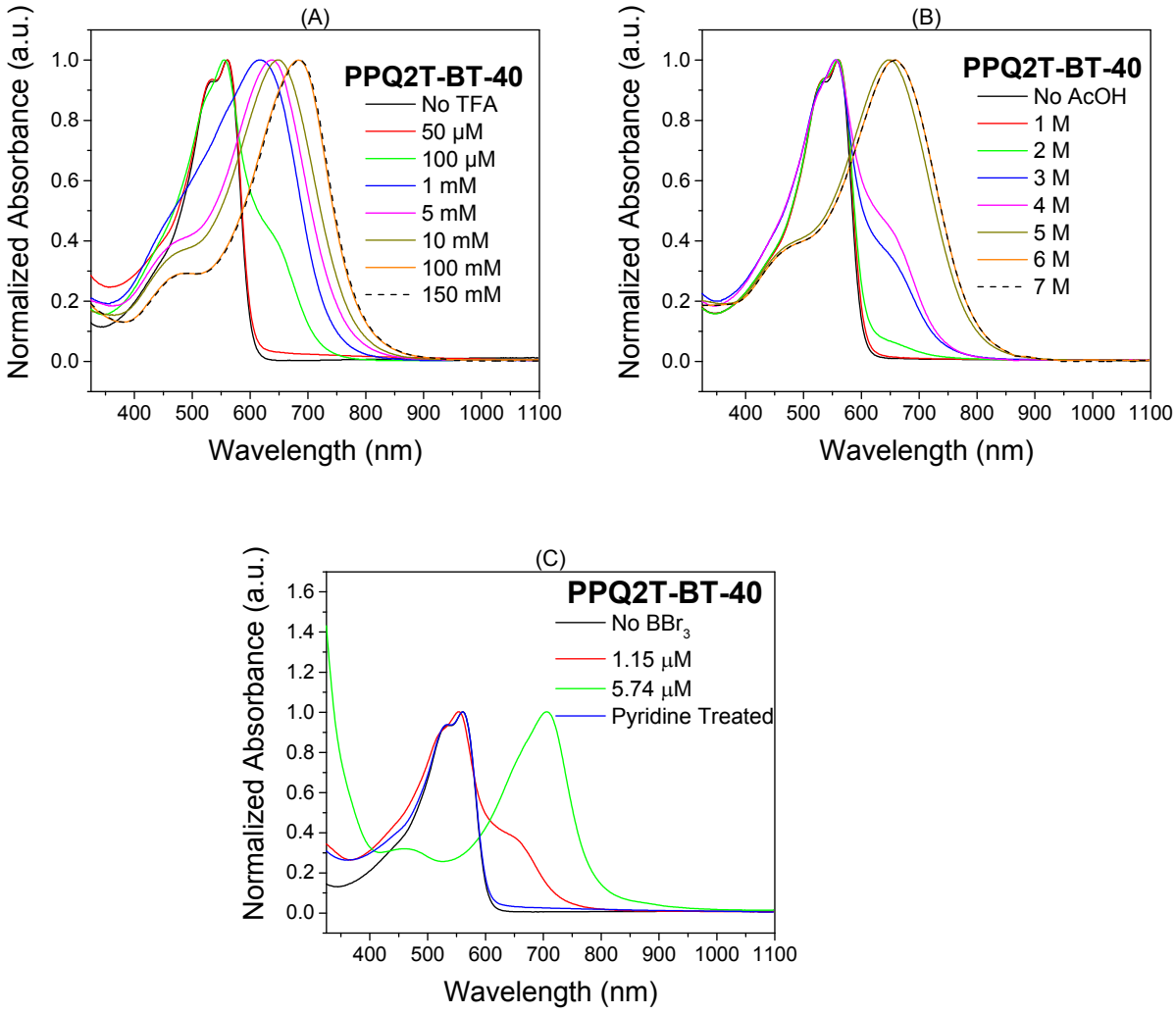

Fig. S11 UV-Vis-NIR absorption spectra of **PPQ2T-BT-40** in chlorobenzene with various concentrations of TFA (A), AcOH (B), and BBr_3 (C), respectively, measured under nitrogen with a molar concentration of the polymer repeat unit at ~1×10^{-5} M. λ_{max} values are listed in Table S2.

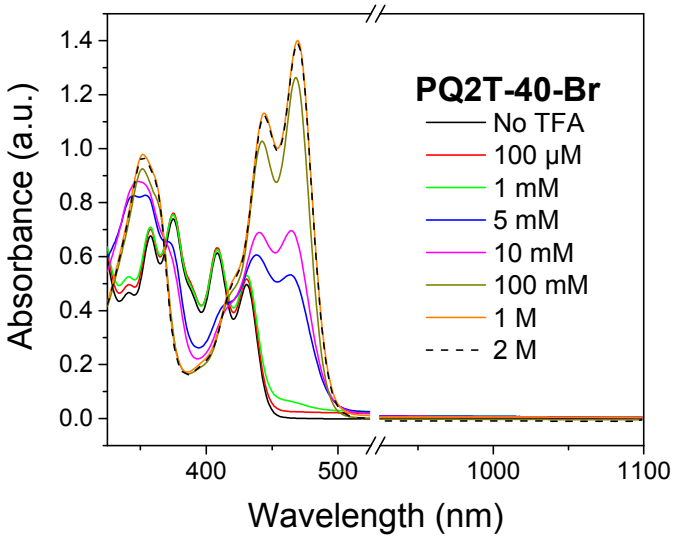

Fig. S12 UV-VIS absorption spectra of **PQ2T-40-Br** in chlorobenzene with various concentrations of TFA measured under nitrogen with a molar concentration of ~1×10^{-5} M.

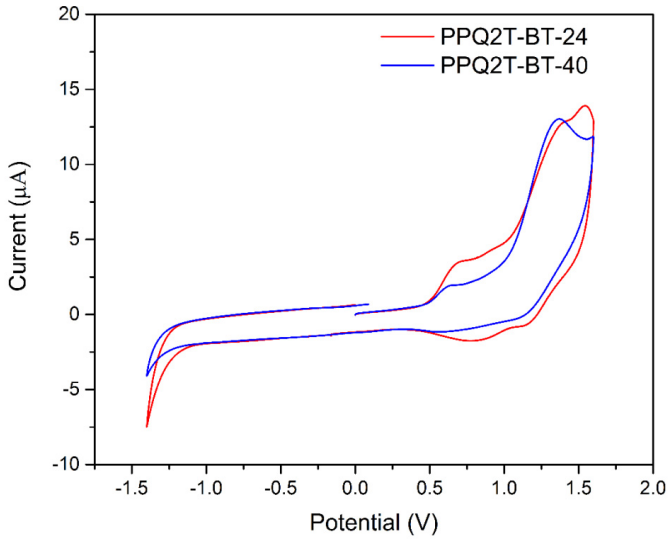

Fig. S13 Cyclic voltammograms of polymers in a 0.1 M tetrabutylammonium hexafluorophosphate solution in anhydrous acetonitrile at a scan rate of 50 mV s^{-1}.

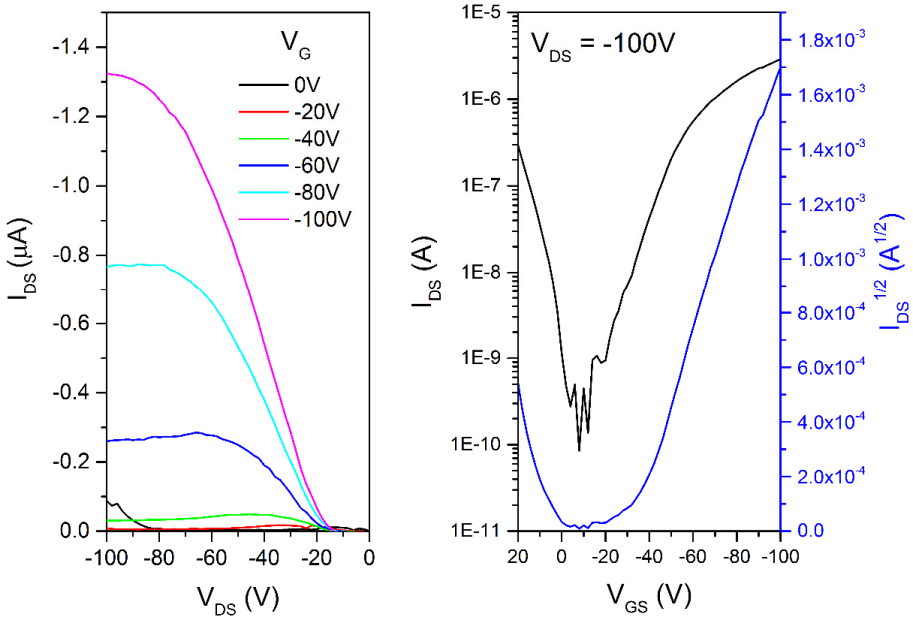

Fig. S14 Output and transfer curves of an OTFT device based on a thin film of **PPQ2T-BT-40** annealed at 250 °C. Device dimensions: channel length (L) = 30 μm; channel width (W) = 1000 μm.

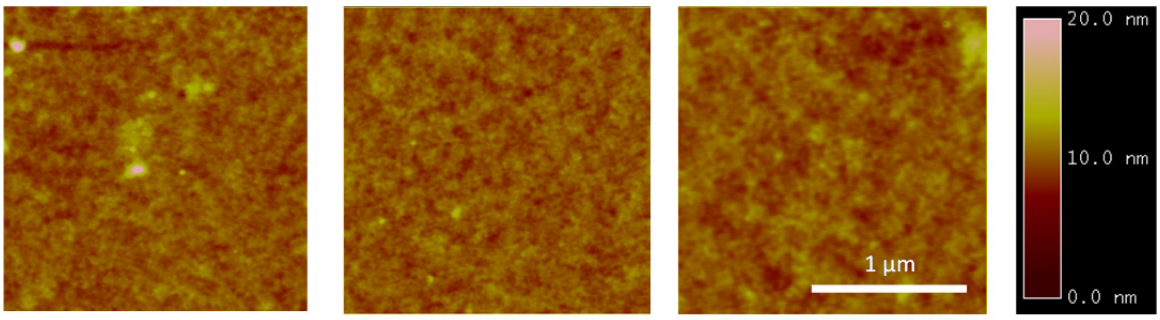

Fig. S15 AFM images (2 μm × 2 μm each) of **PPQ2T-BT-24** thin films on SiO_2/Si substrates annealed at different temperatures. The root mean square (RMS) roughnesses of **PPQ2T-BT-24** were determined to be less than 1 nm for all annealed temperatures.

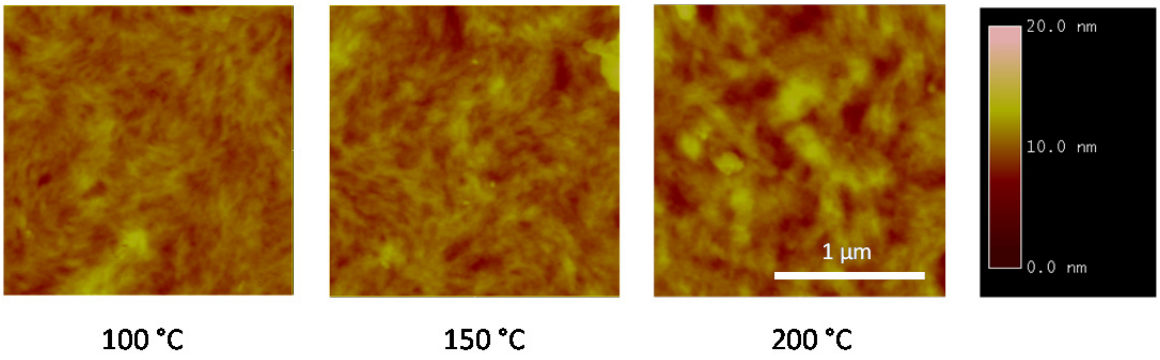

Fig. S16 AFM images (2 µm × 2 µm each) of **PPQ2T-BT-40** thin films on SiO_2/Si substrates annealed at different temperatures. The RMS roughnesses of **PPQ2T-BT-40** are 1.87 (100 °C), 2.24 (150 °C), and 2.93 nm (200 °C).

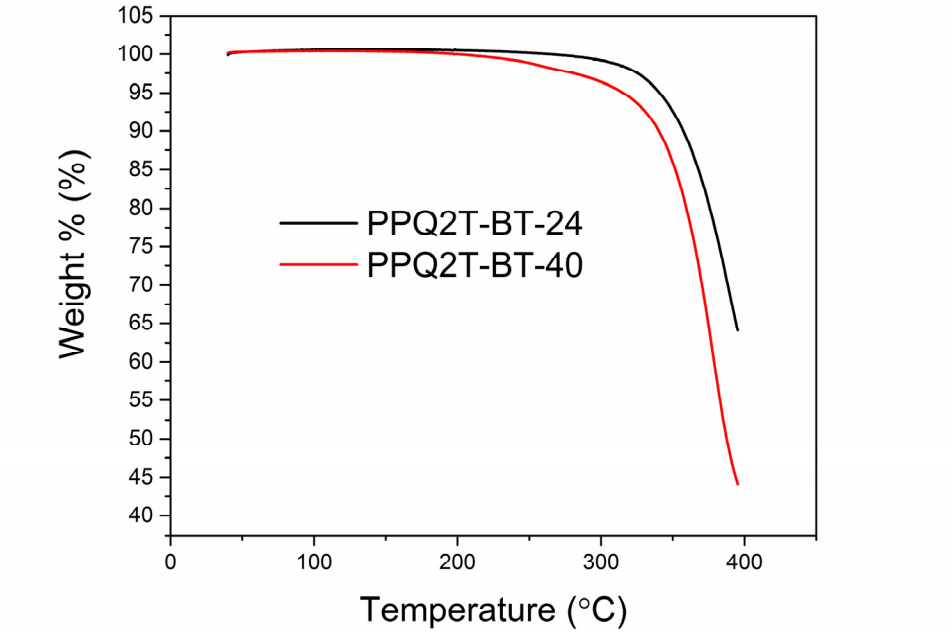

Fig. S17 TGA curves of **PPQ2T-BT-24** and **PPQ2T-BT-40** with a heating rate of 10 °C min^{-1} under nitrogen.

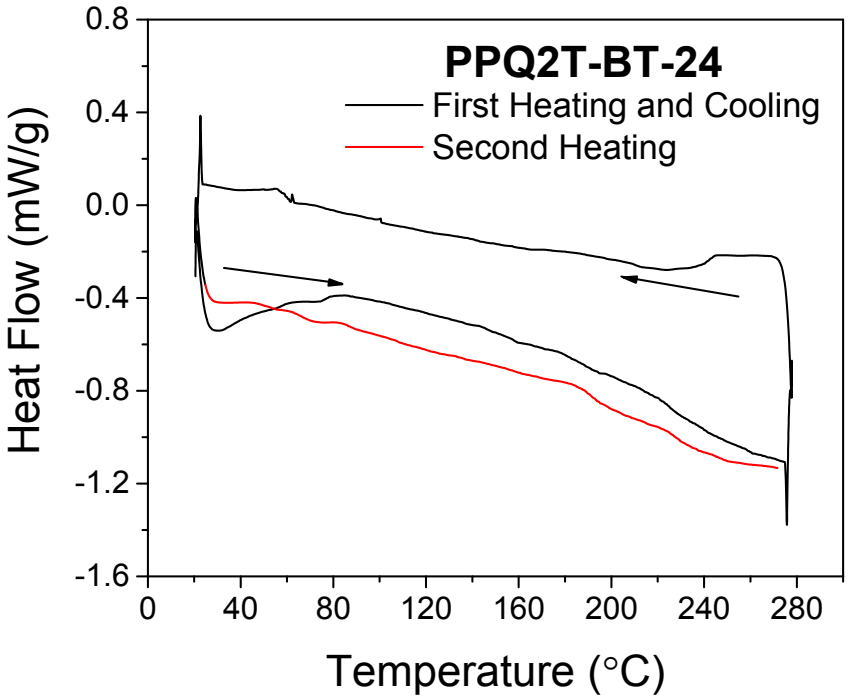

Fig. S18 DSC thermogram of **PPQ2T-BT-24** at a rate of 20 °C min^{-1} under nitrogen.

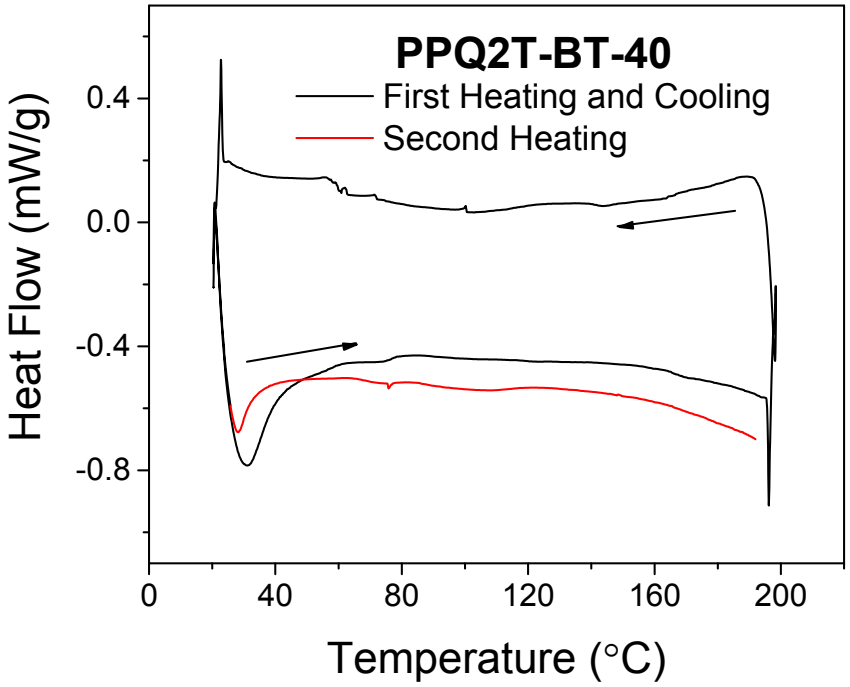

Fig. S19 DSC thermogram of **PPQ2T-BT-40** at a rate of 20 °C min^{-1} under nitrogen.

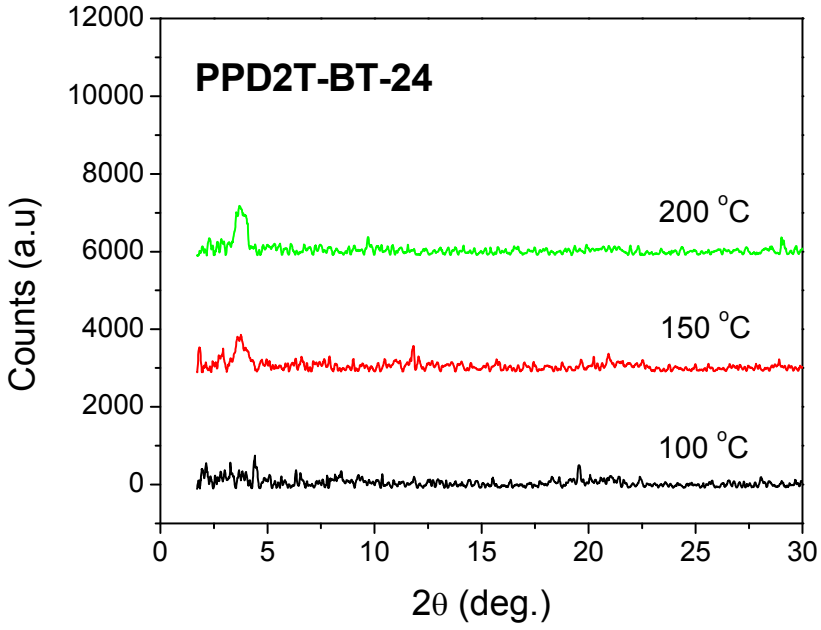

Fig. S20 Reflection XRD diagram of **PPQ2T-BT-24** thin films (~35 nm) spin-coated on dodecyltrichlorosilane-modified SiO_2/Si substrates and annealed at different temperatures with Cu Kα radiation (λ = 0.15406 nm).

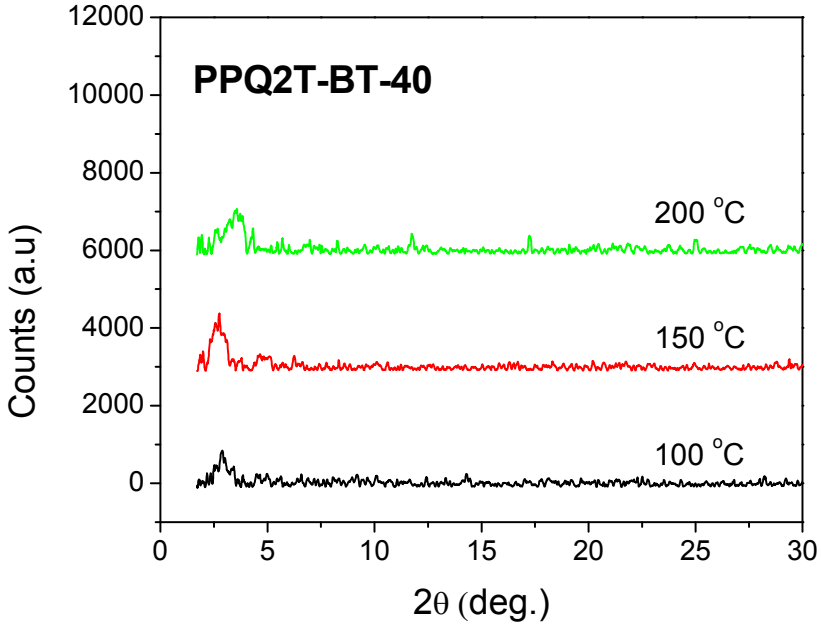

Fig. S21 Reflection XRD diagram of **PPQ2T-BT-40** thin films (~35 nm) spin-coated on dodecyltrichlorosilane-modified SiO_2/Si substrates and annealed at different temperatures with Cu Kα radiation (λ = 0.15406 nm).

Table S1 The summary of OTFT performance of **PPQ2T-BT-24** and **PPQ2T-BT-40**.

Polymer	Annealing temperature (°C)	Hole mobility[a] (10^{-3} cm^2 V^{-1} s^{-1})	Average V_{th} (V)	I_{on} / I_{off}
PPQ2T-BT-24	100	3.42 (3.21 ± 0. 15)	-26.52	~10^3
	150	4.68 (4.49 ± 0. 18)	-27.20	~10^3
	200	5.88 (5.50 ± 0. 28)	-29.15	~10^3
	250	6.43 (5.86 ± 0. 36)	-28.76	~10^3
	300	3.80 (3.43 ± 0. 30)	-23.45	~10^3
PPQ2T-BT-40	100	1.37 (0.86 ± 0. 31)	-15.52	~10^3
	150	2.42 (1.90 ± 0. 75)	-25.43	~10^3
	200	2.97 (2.61 ± 0. 45)	-30.35	~10^5
	250	3.59 (3.12 ± 0. 49)	-30.43	~10^5
	300	3.49 (3.20 ± 0. 21)	-24.30	~10^4

[a] The maximum (average ± standard deviation) mobility was calculated from the saturated regime of at least five devices for each condition.

Table S2 The summary of UV-Vis absorption of various acids for **PPQ2T-BT-24**, **PPQ2T-BT-40**, and **PDQT-24**.

Polymer	TFA		AcOH		BBr_3	
	Conc.	λ_{max}, nm	Conc.	λ_{max}, nm	Conc.	λ_{max}, nm
PPQ2T-BT-24	0	528	0	528	0	528
	10 μM	543	1 M	530	1 μM	533(sh)
	100 μM	545	2 M	536(sh)		
	1 mM	588	3 M	626		
	5 mM	622	4 M	635		
	10 mM	672	5 M	634		
	100 mM	673			6 μM	673
PPQ2T-BT-40	0	562	0	562	0	562
	10 μM	562	1 M	561	1 μM	554(sh)
	100 μM	556	2 M	560		
	1 mM	618	3 M	556(sh)		
	5 mM	638	4 M	556(sh)		
	10 mM	650	5 M	649		
	100 mM	685	6 M	659		
	150 mM	686	7 M	659	6 μM	707
PDQT-24	0	781				
	10 μM	781				
	100 μM	781				
	1 mM	784				
	5 mM	788				
	10 mM	793				
	100 mM	801				
	150 mM	801				

References

1 M. J. Frisch, G. W. Trucks, H. B. Schlegel, G. E. Scuseria, M. A. Robb, J. R. Cheeseman, G. Scalmani, V. Barone, B. Mennucci, G. A. Petersson, H. Nakatsuji, M. Caricato, X. Li, H. P. Hratchian, A. F. Izmaylov, J. Bloino, G. Zheng, J. L. Sonnenberg, M. Hada, M. Ehara, K. Toyota, R. Fukuda, J. Hasegawa, M. Ishida, T. Nakajima, Y. Honda, O. Kitao, H. Nakai, T. Vreven, J. A. Montgomery Jr., J. E. Peralta, F. Ogliaro, M. J. Bearpark, J. Heyd, E. N. Brothers, K. N. Kudin, V. N. Staroverov, R. Kobayashi, J. Normand, K. Raghavachari, A. P. Rendell, J. C. Burant, S. S. Iyengar, J. Tomasi, M. Cossi, N. Rega, N. J. Millam, M. Klene, J. E. Knox, J. B. Cross, V. Bakken, C. Adamo, J. Jaramillo, R. Gomperts, R. E. Stratmann, O. Yazyev, A. J. Austin, R. Cammi, C. Pomelli, J. W. Ochterski, R. L. Martin, K. Morokuma, V. G. Zakrzewski, G. A. Voth, P. Salvador, J. J. Dannenberg, S. Dapprich, A. D. Daniels, Ö. Farkas, J. B. Foresman, J. V. Ortiz, J. Cioslowski and D. J. Fox, *Gaussian 09 Revision D.01*, Gaussian, Inc., Wallingford, CT, USA, 2009.